The G1/S transition is promoted by Rb degradation via the E3 ligase UBR5

Shuyuan Zhang[1], Lucas Fuentes Valenzuela[1], Evgeny Zatulovskiy[1], and Jan M. Skotheim[1,2,*]

[1]Department of Biology, Stanford University, Stanford, CA 94305
[2]Chan Zuckerberg Biohub, San Francisco, CA 94158
[*]Address correspondence to skotheim@stanford.edu

Abstract

Mammalian cells make the decision to divide at the G1/S transition in response to diverse signals impinging on the retinoblastoma protein Rb, a cell cycle inhibitor and tumor suppressor. Rb is inhibited by two parallel pathways. In the canonical pathway, cyclin D-Cdk4/6 kinase complexes phosphorylate and inactivate Rb. In the second, recently discovered pathway, Rb's concentration decreases during G1 through an unknown mechanism. Here, we found that regulated protein degradation via the E3 ubiquitin ligase UBR5 is responsible for Rb's concentration drop in G1. *UBR5* knockout cells have increased Rb concentration in early G1, exhibited a lower G1/S transition rate, and are more sensitive to inhibition of Cdk4/6. This last observation suggests that UBR5 inhibition can strengthen the efficacy of Cdk4/6 inhibitor-based cancer therapies.

One-Sentence Summary: The E3 ligase UBR5 progressively reduces the concentration of the retinoblastoma protein Rb during G1 to drive proliferation.

Main Text

The decision to divide often takes place in the G1 phase of the cell cycle and occurs in response to diverse input signals. Once taken, the decision to initiate DNA replication and divide is difficult to reverse despite changes to the input signals (*1*, *2*). From a molecular point of view, the commitment point at the G1/S transition in response to growth signals corresponds to the hyper-phosphorylation and inactivation of the transcriptional inhibitor Rb, the retinoblastoma protein (*1*, *3*, *4*). Hyper-phosphorylation of Rb frees the activating E2F transcription factors to drive expression of the cyclins E and A, which mostly form complexes with the cyclin-dependent kinase Cdk2. Active cyclin E/A-Cdk2 complexes then maintain Rb hyper-phosphorylation so that E2F-dependent transcription remains active (*5*). While the molecular basis of the commitment point to cell division is increasingly well understood, we know much less about how the upstream growth and differentiation input signals transmit quantitative information to the decision point.

Activating signals promoting the G1/S transition operate through at least two parallel pathways. First, growth factors initiate signals that increase the expression of cyclin D (*6*), which primarily forms a complex with the cyclin-dependent kinases Cdk4 and Cdk6 (*7*). Cyclin D-Cdk4/6 complexes then initiate the phosphorylation of Rb, possibly through hypo- or mono-phosphorylation (*8*, *9*), to promote the G1/S transition. A second parallel activating signal operates through the concentration of Rb itself, which we recently found to decrease as cells grow through G1 (*10*, *11*). Thus, the current model is that these two mechanisms cooperate to activate E2F-dependent transcription and initiate the cell cycle. Namely, cyclin D-dependent Rb hypo-phosphorylation shifts the dissociation constant (K_d) of Rb with E2F so that the decreasing Rb concentration can drop below K_d to release active E2F. Following the G1/S transition, Rb's concentration increases during S/G2/M to reset for the next cell cycle. Although several molecular mechanisms underlying cyclin D synthesis and Rb phosphorylation by cyclin D-Cdk4/6 have been elucidated (*8*, *12*), the molecular mechanism underlying the decrease in Rb concentration through G1 is unknown.

Here, we sought to determine the molecular mechanisms underlying Rb's concentration decrease through G1 (Fig. 1A), an important signal triggering the G1/S transition. We found that Rb is targeted for degradation in G1 by the E3 ligase UBR5. At the G1/S transition, Rb is stabilized by hyper-phosphorylation so that its concentration recovers for the next G1 phase. Disruption of this G1 Rb degradation mechanism decreases the G1/S transition rate and sensitizes cells to chemical inhibition of the parallel pathway based on Cdk4/6 activity.

Rb concentration dynamics are regulated by degradation

63 During early- to mid-G1 phase, the concentration of Rb protein continuously decreases to
64 promote cell cycle entry (*10*)(Fig. 1B, Fig. S1A). Then, in late G1, the Rb concentration begins
65 its recovery back to the initial concentration. This transition point in mid/late-G1 is marked by an
66 increase in Cdk activity as assessed by the nuclear translocation of an HDHB-based sensor (*1*,
67 *13*). These dynamics are relatively unique, as the concentrations of other G1/S pathway
68 components remain constant throughout G1 phase (*10*, *11*). Moreover, a proteomics analysis
69 revealed that Rb concentration changes far exceed those of a typical protein through the cell
70 cycle (*14*). The dilution of Rb in G1 is an important input to the decision to divide as the Rb
71 concentration is anti-correlated with the G1/S transition rate (*10*), and increasing the overall Rb
72 concentration sensitizes cells to treatment by Cdk4/6 inhibitors (Fig. 1C, Fig. S1B).
73
74 To identify the mechanism regulating Rb concentration dynamics through the cell cycle, we
75 examined both the synthesis and degradation of Rb protein in different cell cycle phases. We
76 measured the mRNA concentration of *RB1* in different cell cycle phases by using flow cytometry
77 to sort HMEC (telomerase-immortalized human mammary epithelial) cells expressing FUCCI
78 (*15*) cell cycle reporters into G1 and S/G2 populations. We then performed qPCR or mRNA-Seq
79 to measure *RB1* mRNA expression. The results showed that the *RB1* mRNA concentration did
80 not significantly increase in S/G2 phase (Fig. 1D, Fig. S1C). We found a similar result when
81 calculating *RB1* mRNA concentrations in different cell cycle phases using a published
82 MERFISH dataset (*16*) (Fig. S1D). This indicates that Rb concentration dynamics are controlled
83 by post-transcriptional mechanisms. To further investigate the synthesis dynamics of Rb protein,
84 we measured the translation efficiency of *RB1* mRNA by performing a RIP (RNA-binding
85 protein immunoprecipitation) assay against the translation initiation factor eIF4E. The relative
86 translation efficiency is calculated by dividing the bound fraction of *RB1* with the bound fraction
87 of housekeeping genes (*Actin* and *GAPDH*). Using this method, we found the relative translation
88 efficiency of *RB1* was similar in sorted G1 and S/G2 cells as well as in asynchronously dividing
89 and G1 arrested cells (Palbociclib treatment) (Fig. 1E, Fig. S1E). Taken together, our data
90 indicate that Rb synthesis is not primarily responsible for its cell cycle dynamics.
91
92 Having found that Rb's cell cycle dynamics were not primarily due to transcription or translation
93 mechanisms, we next sought to test if degradation mechanisms were responsible. To do this, we
94 utilized a doxycyclin (Dox)-inducible system in which cells conditionally express Clover-
95 3xFlag-tagged Rb (*TRE-Clover-3xFlag-Rb*) or Clover-NLS (*TRE-Clover-NLS*) upon Dox
96 treatment (1μg/mL). After 36h of Dox treatment, we withdrew Dox and monitored the decrease
97 of the Clover fluorescence signal using live cell imaging (Fig. S1F). Since the cells also express
98 a FUCCI cell cycle marker, we can separately assess protein degradation taking place in G1 and
99 S/G2 phases of the cell cycle (Fig. 1F, Fig. S1F). By fitting the degradation traces using a simple
100 exponential decay function, we obtained the half-life of Clover-3xFlag-Rb protein in different
101 cell cycle phases for each cell. Rb half-life in early G1 (median 6.4h; 75% range 5.3h-9.4h) is
102 significantly shorter than it is in S/G2 (median 37.3h, 75% range 29.2h-45.4h) (Fig. 1F). The Rb

103 tag location does not affect its half-life since a C-terminally tagged Rb protein (Rb-3xFlag-
104 Clover) behaved similarly to the N-terminally tagged version (Fig. 1G). The changing Rb
105 stability through the cell cycle was specific to Rb since a short-lived Clover-NLS protein and
106 stable Clover-NLS protein both had half-lives that did not change through the cell cycle (Fig.
107 1G; Fig. S1G, H). Thus, these results suggest a model where the Rb protein's cell cycle
108 dynamics are due to its degradation in G1 and stabilization at the G1/S transition.
109
110 Having established that the regulation of Rb stability is most likely responsible for its cell cycle
111 dynamics, we sought to test if this differential degradation of Rb is sufficient to give rise to the
112 observed dynamics. To do this, we generated a mathematical model where only the half-life of
113 the Rb protein changed through the cell cycle, while the synthesis rate remained constant (see
114 methods). This simple model revealed that regulated degradation was sufficient to generate the
115 cell-cycle dependent Rb concentration dynamics we observed, while the modest upregulation in
116 the synthesis rate was insufficient (Fig. 1H). Thus, our findings imply that cell cycle-dependent
117 regulation of Rb stability is responsible for its cell cycle dynamics (Fig. 1I).
118
119 **Rb is stabilized via phosphorylation by Cdk**
120
121 Having found that Rb is stabilized at the G1/S transition, we next sought to identify the
122 molecular mechanism. One of the most prominent molecular changes occurring at the G1/S
123 transition is the phosphorylation of Rb by cyclin-Cdk complexes. We therefore sought to
124 examine how Rb phosphorylation affected its half-life. To do this, we first stained asynchronous
125 HMEC cells with phospho-Rb (S807/811) and total Rb antibodies. We then calculated the Rb
126 concentration in the low phospho-Rb G1 population (low pRb G1), the high phospho-Rb G1
127 population (high pRb G1), and the S/G2 population. The Rb concentration is lower in early G1
128 when it is not hyper-phosphorylated and then begins to recover in late G1, when Rb is
129 phosphorylated (Fig. 2A). Similar results were obtained when G1 was partitioned into early and
130 late phases using a live-cell Cdk activity sensor based on the C-terminal part of Rb (*17*) (Fig.
131 S2A). These immunofluorescence data support the model where the Rb concentration decrease
132 in G1 phase is reversed upon its phosphorylation. Consistently, when cells are arrested in G1 by
133 treating them with the Cdk4/6 inhibitor Palbociclib (1μM) for 24 hours, the Rb protein
134 concentration drops by ~75% (Fig. 2B) even though the mRNA concentration is only reduced by
135 ~15% (Fig. S2B). This is consistent with published results showing significant Rb protein drops
136 when cells are exposed to Cdk4/6 inhibitors(*18*). Furthermore, in cells expressing a Dox-
137 inducible Clover-3xFlag-Rb protein, Palbociclib treatment led to a significant decrease in the
138 concentration of this ectopically expressed protein but not the corresponding mRNA (Fig. S2C).
139 Taken together, these data suggest that the phosphorylation of Rb by Cdk mediates its
140 stabilization.
141

142 To further investigate how Rb phosphorylation on different Cdk phosphorylation sites affect its
143 half-life, we used the Dox-inducible system to express a series of Rb variants in which the Cdk
144 phosphorylation sites were either substituted with non-phosphorylatable alanines or with
145 phospho-mimetic double glutamic acid residues (EE) (*19*) (Fig. S2D). For both mutant series, we
146 extended the number of mutant sites from either the N- or C-terminus so that different mutants
147 covered different parts of the protein (Fig. S2D). If Cdk phosphorylation stabilizes Rb, then the
148 phospho-mutants (S/T to A) should exhibit a reduced half-life in S/G2, and the phospho-mimetic
149 mutants (S/TP to EE) should exhibit increased half-life in early G1. Our results are consistent
150 with this hypothesis (Fig. 2C, D; Fig. S2E, F). It is worth noting that the C-terminal alanine-
151 mutants also had a more severe cell cycle arrest phenotype (Fig. S3A). This is likely because the
152 alanine mutants do not allow the phosphorylation of C-terminal residues to disrupt Rb's
153 interaction with E2F-DP (*12*, *17*, *20*, *21*). On the other hand, the phospho-mimetic mutants did
154 not demonstrate significant cell cycle defects (Fig. S3B), likely because these Rb mutants are
155 partially or entirely unable to bind and inhibit E2F. In addition, the introduction of phospho-
156 mimetic mutations resulted in a smaller Rb concentration decrease in cells arrested in G1 using
157 Palbociclib (Fig. S2C; Fig. S3C, D).
158
159 Interestingly, our mutational analysis did not reveal any particular phosphorylation sites that
160 predominantly regulated Rb's half-life (Fig. 2E, F; Fig. S2F; Fig. S3C, D). Instead, the degree of
161 Rb stabilization – *i.e.*, the ratio between early G1 and S/G2 half-lives – correlated with the total
162 number of phospho-mimetic sites. This shows that many different phosphorylation sites
163 contribute to Rb stability. We note that Rb14EE exhibited reduced half-lives for both early G1
164 and S/G2 phases, which is likely due to the additional SP230EE mutation destabilizing the
165 protein via another mechanism. However, the difference between early G1 and S/G2 half-lives in
166 Rb14EE is the smallest (Fig. S2F). Collectively, these results support the hypothesis that hyper-
167 phosphorylation by Cdk stabilizes Rb in late G1 (Fig. 2G).
168
169 **The degradation of un-phosphorylated Rb is mediated by the E3 ubiquitin ligase UBR5**
170
171 After establishing that Rb is stabilized by phosphorylation at the G1/S transition, we next sought
172 to identify the underlying molecular mechanism. To do this, we first tested whether Rb is
173 degraded through the ubiquitin-proteasome system by treating cells with three commonly used
174 inhibitors of different components of this degradation system: Bortezomib inhibits the
175 proteasome; TAK243 inhibits the ubiquitin activating enzyme (E1); and MLN4924 inhibits the
176 NEDD8-activating enzyme that activates the Cullin (CUL)-RING E3 ubiquitin ligases (*22*, *23*).
177 We treated asynchronously growing HMEC cells with these inhibitors for 5 hours, and then
178 immunostained the cells using antibodies for pRb(S807/811) and total Rb. TAK243 and
179 Bortezomib treatments increased the Rb concentration in the low pRb G1 populations to a level
180 similar to that in the high pRb G1 population, but MLN4924 did not (Fig. 3A, Fig. S4A). RPE-1
181 cells (telomerase immortalized retinal pigment epithelium cells) behaved similarly to HMEC

182 cells in that only TAK243 and Bortezomib treatments increased the Rb concentration in the low
183 pRb G1 population (Fig. S4B). To further confirm that the phosphorylation status determines Rb
184 degradation through the ubiquitin-proteasome system, we treated cells that were induced to
185 express un-phosphorylatable Rb (Clover-3xFlag-RbΔCDK) or phospho-mimetic Rb (Clover-
186 3xFlag-Rb14EE) with the three degradation inhibitors discussed above. The concentration of
187 RbΔCDK is elevated by TAK243 and Bortezomib, but not MLN4924, and the concentration of
188 Rb14EE does not increase following treatment by any of the three inhibitors (Fig. 3B). We also
189 confirmed the enhanced ubiquitination of RbΔCDK by pulling down Clover-3xFlag-RbΔCDK
190 and blotting for ubiquitin. RbΔCDK was more ubiquitinated than WT Rb (Fig. S4C). Altogether,
191 these data suggest that un-phosphorylated Rb is degraded in G1 through the ubiquitin-
192 proteasome system, but not by the Cullin (CUL)-RING E3 ligases.
193
194 There have been several previous studies of Rb degradation mechanisms that have identified
195 some E3 ligases (*18*, *24–31*). For example, MDM2 may mediate Rb degradation via its central
196 acidic domain (*24*, *25*, *29*). The human papilloma virus (HPV) E7 protein can bind Rb and
197 induce its degradation (*28*), which is mediated by protease cleavage at Lys810 (*26*). More
198 recently, Cdk4/6 inhibition was found to promote Rb degradation through βTrCP1-mediated
199 ubiquitination (*18*). To test if these E3 ligases were responsible for the observed cell cycle
200 dynamics of Rb, we examined the effect of knocking them down on the concentration of un-
201 phosphorylatable Rb (Clover-3xFlag-RbΔCDK) and phospho-mimetic Rb (Clover-3xFlag-
202 Rb14EE). If an E3 were responsible for Rb's cell cycle dynamics, we would expect to see an
203 increase in the concentration of Clover-3xFlag-RbΔCDK but not of Clover-3xFlag-Rb14EE.
204 None of the knockdowns exhibited this predicted phenotype (Fig. S5A). Even through some of
205 the knockdowns affected the overall Rb concentration, this effect was not specific for
206 unphosphorylated Rb and therefore could not explain Rb's cell cycle dynamics. Similarly, we
207 performed the same set of knockdowns in cells arrested in G1 using Palbociclib and did not find
208 any specific increase in the concentrations of un- or hypo-phosphorylated Rb (Fig. S5B-G). This
209 implies that there must be some additional E3 ligase responsible for the phosphorylation-
210 dependent degradation of Rb.
211
212 To identify the E3 ligases mediating the degradation of un-phosphorylated Rb, we set up an
213 siRNA screen. We used a customized siRNA library that included the previously published E3
214 ligases for Rb, some nuclear localized E3s (according to UniProt), and some additional genes
215 predicted to be E3 ligases for Rb (http://ubibrowser.bio-it.cn/ubibrowser_v3/) (Fig. 3C). HMEC
216 cells inducibly expressing Clover-3xFlag-RbΔCDK or Clover-3xFlag-Rb14EE were transfected
217 with the siRNA library. 48 hours later, cells were fixed and imaged. The concentration of
218 Clover-3xFlag-Rb variants was measured in each treatment and its fold change over non-
219 transfected cells was calculated. As positive controls, we included the ubiquitin-proteasome
220 system inhibitors TAK243 and Bortezomib. As expected, TAK243 and Bortezomib only
221 increased the concentration of RbΔCDK but not Rb14EE (Fig. 3D; Fig. S6A, B). From this

222 screen, we only identified UBR5 as specifically targeting unphosphorylated Rb for degradation.
223 UBR5 is a verified E3 ubiquitin ligase belonging to the HECT family known to play roles in
224 transcription and the DNA damage response (*32–35*) (Fig. 3D; Fig. S6A, B). However, Rb has
225 never been reported to be a substrate of UBR5.
226
227 To confirm that UBR5 is the main E3 ligase targeting un-phosphorylated Rb, we first performed
228 another siRNA screen with a different siRNA library containing UBR5 and 16 other E3 genes
229 from the first library as well as the rest of the nuclear localized E3 genes not included in the first
230 screen. We also included several E1 and E2 genes (Fig. 3C). This second siRNA screen also only
231 identified UBR5 (Fig. 3D; Fig. S6B-D). We then validated UBR5 as a hit using another two
232 independent siRNAs against UBR5. Knockdown of UBR5 in HMEC cells led to the
233 accumulation of un/hypo-phosphorylated Rb after Palbociclib treatment, as measured by both
234 immunoblot and immunostaining (Fig. 3E-G; Fig. S7A). We also measured the half-life of Rb
235 following UBR5 knockdown using live-cell imaging and found that Rb was degraded about
236 twice as slowly in early G1, but not in S/G2, as compared to the control siRNA (Fig. 3H).
237 Moreover, we examined the effect of knocking down UBR5 on HMEC cells expressing
238 endogenously tagged Rb (*RB1-3xFLAG-Clover-sfGFP*)(*10*). Following *UBR5* knockdown, the
239 concentration of Rb does not decrease in early G1, but is instead kept relatively constant (Fig.
240 S7B). To further confirm that the degradation of un-phosphorylated Rb by UBR5 is not cell line
241 or cell type specific, we also examined epithelial RPE-1 cells as well as HLF (primary human
242 lung fibroblast) and T98G (glioblastoma-derived fibroblast-like) cells. All of them showed that
243 UBR5 knockdown increased concentrations of un- and hypo-phosphorylated Rb in Palbociclib-
244 treated cells (Fig. S7C-E).
245
246 To test if UBR5 mediated Rb degradation *in vivo*, we examined its effect in the mouse liver
247 using the *Fah-/-* system(*36*, *37*). In the *Fah-/-* system, deletion of the *Fah* gene causes toxin
248 accumulation in hepatocytes that will lead to hepatocyte death. Toxin accumulation can be
249 prevented by treating mice with NTBC (2-(2-nitro-4-trifluoromethylbenzoyl)-1,3-
250 cyclohexanedione)(*37*). When NTBC is withdrawn, cells expressing exogenous *Fah*, introduced
251 by injecting *Fah*+ transposons, will clonally expand to repopulate the injured liver (*37*) (Fig. 3I).
252 Importantly, other genetic elements, such as Cas9 and gRNA, can be added to the *Fah*
253 transposon so that they are co-integrated into some hepatocyte genomes. To knock out *Ubr5* in
254 some hepatocytes, we modified an *Fah* transposon plasmid (*38*) and delivered *Fah-P2A-Cas9-*
255 *sgUbr5* or *Fah-P2A-Cas9-sgNT* (non-targeting) transposons and the SB100 transposase into
256 *Fah*−/− mice via hydrodynamic transfection. 8 weeks after injection, when the liver was almost
257 fully repopulated with *Fah*+ cells, we isolated the hepatocytes, plated them, and performed
258 immunostaining or immunoblots (Fig. 3I). Consistent with the results from human cell lines,
259 knocking out *Ubr5* increased Rb concentrations in mouse hepatocytes where Rb was not hyper-
260 phosphorylated (low pRb) (Fig. 3J, Fig. S7F). The results from *Fah-/-* *in vivo* model further

261 supports our conclusion that the E3 ligase UBR5 targets un-phosphorylated Rb for degradation
262 in G1 (Fig. 3K).
263
264 Our results here give insight into why previous studies reported other E3s targeting Rb. First, any
265 E3 whose knockdown results in a cell cycle phenotype would be predicted to have an effect on
266 Rb concentration. Second, after finding Rb dynamics were driven by the degradation of un- or
267 hypo-phosphorylated Rb in G1 phase, we sought to find E3s that specifically targeted the un-
268 phosphorylatable RbΔCDK protein, but not the phospho-mimetic Rb14EE protein. We did find a
269 significant increase in both RbΔCDK and Rb14EE when the E3 MDM2 was knocked down, and
270 possibly very modest effects when other reported E3s were knocked down (Fig. S5A; Fig. S6A).
271 This suggests that these different E3s operate in different cell types or contexts, but are not
272 responsible for Rb's cell cycle dynamics.
273
274 **UBR5 and Cdk4/6 drive parallel pathways promoting the G1/S transition**
275
276 It is becoming increasingly clear that there are two distinct pathways driving the G1/S transition
277 that both operate through Rb. First, the canonical Cdk-phosphorylation pathway through which
278 cyclin D-Cdk4/6 complexes phosphorylate and inhibit Rb, and second, the Rb-degradation
279 pathway that drives down the concentration of Rb in G1 phase. One prediction from this parallel
280 pathway model is that cells lacking the Rb-degradation pathway should be more sensitive to
281 inhibition of the remaining Rb-phosphorylation pathway. We can now test this prediction
282 because we identified UBR5 as the E3 ligase targeting un-phosphorylated Rb in G1. To do this,
283 we first generated clonal cell lines lacking *UBR5* from HMEC cells using CRISPR/Cas9. We
284 randomly picked three *UBR5 WT* clones and three *UBR5 KO* clones for analysis (Fig. 4A).
285 *UBR5 KO* cells exhibited higher Rb concentrations in low pRb G1 cells (Fig. 4B, C; Fig. S8).
286 Moreover, *UBR5 KO* cells also exhibited both higher endogenous Rb concentrations and higher
287 exogenous Clover-3xFlag-Rb concentrations following Palbociclib treatment to arrest cells in G1
288 (Fig. S8; Fig. S9A, B), as well as an increased Rb half-life in early G1 (Fig. S9C). These
289 knockout lines therefore exhibited all the same effects we observed in our earlier knockdown
290 experiments shown in Fig. 3.
291
292 Having established *UBR5 KO* cells, we are now in a position to test the parallel pathway model
293 prediction that cells lacking the Rb-degradation pathway are more sensitive to inhibition of the
294 Rb-phosphorylation pathway. To do this, we treated *UBR5 WT* and *UBR5 KO* cells with the
295 Cdk4/6 inhibitor Palbociclib for 72 hours and then measured cell numbers. Since different clonal
296 cell lines had different proliferation rates to begin with (Fig. S10A), we normalized the cell
297 numbers of Palbociclib treated cells to the cell numbers in the DMSO control treatment for each
298 clonal cell line. Moreover, this normalization also accounts for the slower growth rates of *UBR5*
299 *KO* cells (Fig. S10A) that are likely due to the dysregulation of other UBR5 substrates. As
300 predicted by the parallel pathway model, *UBR5 KO* cells are more sensitive to Palbociclib

301 treatment than *UBR5 WT* cells (Fig. 4D, Fig. S10A). To further determine the proliferation status
302 of *UBR5 WT* and *KO* cells, we also stained the cells with phospho-Rb antibodies following
303 DMSO or Palbociclib treatments. As expected, a significantly higher proportion of *UBR5 WT*
304 cells were progressing through the cell cycle (as indicated by cells having hyper-phosphorylated
305 Rb) compared to *UBR5 KO* cells, again supporting the parallel pathway model (Fig. S10B-D).
306
307 Since UBR5 has other substrates that may also affect cell cycle progression, we wanted to
308 examine if UBR5 KO cells' increased sensitivity to Palbociclib treatment was due to the
309 stabilization of Rb. To test this, we knocked out *RB1* in *UBR5 KO* cells using CRISPR/Cas9
310 (Fig. S11A) and tested their sensitivity to Palbociclib treatment. Knocking out *RB1* in *UBR5 KO*
311 cells completely rescued the increased Palbociclib sensitivity exhibited by *UBR5 KO* cells (Fig.
312 4E; Fig. S11B), suggesting that the effect of UBR5 on the G1/S transition is primarily through
313 the stabilization of Rb. Lastly, to make sure that the effect of UBR5 on cell cycle progression
314 was due to its E3 ligase activity, we added back either wild-type UBR5 or an inactive mutant
315 UBR5 to the *UBR5 KO* cells using the Dox-inducible system (Fig. S11C). The mutant UBR5 has
316 a C2768A mutation in the HECT domain, which kills its catalytic activity (*33*). The expression
317 of WT or mutant UBR5 was induced by Dox, and cells were treated with DMSO or Palbociclib
318 for 72 hours. Adding back UBR5 WT increased the normalized cell number as compared to the
319 no Dox control, whereas adding back the mutant UBR5 did not (Fig. 4F; Fig. S11D, E). This
320 indicates that the E3 ligase activity of UBR5 is essential for its function as a key component of
321 the Rb-degradation pathway driving progression through the G1/S transition.
322
323 **Discussion**
324
325 Two distinct pathways drive the G1/S transition by reducing the activity and amount of the key
326 cell cycle inhibitor Rb: the canonical Cdk-phosphorylation pathway and the Rb-degradation
327 pathway (Fig. 4G). Here, we report that the Rb-degradation pathway is driven by the E3
328 ubiquitin ligase UBR5 and is shut off by Rb hyper-phosphorylation in late G1. However, we do
329 not yet know the mechanism through which UBR5 recognizes Rb. UBR5 likely engages its
330 substrates as a dimer or tetramer, which can target distinct degron linear motifs as indicated by
331 recent cryo-EM structures (*34*, *35*, *39–41*). Since UBR5 is a large multi-domain protein, it is
332 possible that different docking mechanisms can be utilized for engaging different groups of
333 substrates involved in multiple biological processes (*33*, *35*, *40–42*). Interestingly, two recent
334 studies proposed that UBR5 targets its substrates on chromatin (*34*, *35*). This possible preference
335 of UBR5 for chromatin-bound targets might explain the results of our mutational analysis of Rb.
336 Namely, the more tightly an Rb variant is predicted to bind the E2F transcription factor, the more
337 rapidly it is degraded. The stabilization of Rb at the G1/S transition is coincident with its hyper-
338 phosphorylation and subsequent dissociation from the chromatin-bound E2F transcription
339 factors.
340

Components of the canonical Rb-phosphorylation pathway are frequently mutated in cancer and have become targets for therapies (*43*). For example, Cdk4/6 inhibitors in combination with endocrine therapy are used to treat advanced estrogen receptor positive (ER+)/human epidermal growth factor receptor-2 negative (HER2-) breast cancers (*44–46*). However, this application is frequently limited by the intrinsic and acquired therapeutic resistance observed in patients (*47*, *48*). One possible way to improve upon current therapies targeting the Rb-phosphorylation pathway is to also target the Rb-degradation pathway. Namely, since deleting UBR5 sensitizes cells to treatment by Cdk4/6 inhibitors, it is possible that current Cdk4/6 inhibitor-based treatments for breast cancer can be improved by developing novel therapeutics targeting the Rb-degradation pathway through UBR5.

The inability of current therapies to inhibit cell division likely reflects our incomplete knowledge of the signaling pathways involved. During G1 phase, the cell integrates many signals to make tiehe decision to commit to cell division including two separate signaling pathways targeting Rb. The existence of these two parallel pathways explains the ability of some cells to proliferate in the absence of cyclin D-dependent kinase activity (*49–51*). Namely, these cells rely more heavily on the UBR5-Rb degradation pathway than the canonical Cdk4/6 Rb-phosphorylation pathway. In addition to providing such a robust entry to the cell division cycle in a particular cellular context, the existence of parallel pathways regulating the G1/S transition might be due to the different proliferative requirements of diverse cell types (*52*). Different pathways can be independently tuned to precisely calibrate the rate of proliferation required by the myriad cell types and niches of a multicellular organism. Discovering the mechanisms underlying these G1/S regulatory pathways, such as we have here for Rb-degradation, will give insight into both development and disease.

368 **References**
369

370 1. C. Schwarz, A. Johnson, M. Kõivomägi, E. Zatulovskiy, C. J. Kravitz, A. Doncic, J. M.
371 Skotheim, A Precise Cdk Activity Threshold Determines Passage through the Restriction
372 Point. *Mol Cell*. **69**, 253-264.e5 (2018).

373 2. S. D. Cappell, M. Chung, A. Jaimovich, S. L. Spencer, T. Meyer, Irreversible APCCdh1
374 Inactivation Underlies the Point of No Return for Cell-Cycle Entry. *Cell*. **166**, 167–180
375 (2016).

376 3. J. Moser, I. Miller, D. Carter, S. L. Spencer, Control of the Restriction Point by Rb and p21.
377 *Proceedings of the National Academy of Sciences*. **115**, E8219–E8227 (2018).

378 4. A. Zetterberg, O. Larsson, K. G. Wiman, What is the restriction point? *Curr Opin Cell Biol*.
379 **7**, 835–842 (1995).

380 5. S. M. Rubin, J. Sage, J. M. Skotheim, Integrating Old and New Paradigms of G1/S Control.
381 *Mol Cell*. **80**, 183–192 (2020).

382 6. J. T. Winston, W. J. Pledger, Growth factor regulation of cyclin D1 mRNA expression
383 through protein synthesis-dependent and -independent mechanisms. *Mol Biol Cell*. **4**, 1133–
384 1144 (1993).

385 7. A. Fassl, Y. Geng, P. Sicinski, CDK4 and CDK6 kinases: From basic science to cancer
386 therapy. *Science*. **375**, eabc1495 (2022).

387 8. A. M. Narasimha, M. Kaulich, G. S. Shapiro, Y. J. Choi, P. Sicinski, S. F. Dowdy, Cyclin D
388 activates the Rb tumor suppressor by mono-phosphorylation. *eLife*. **3**, e02872 (2014).

389 9. I. Sanidas, R. Morris, K. A. Fella, P. H. Rumde, M. Boukhali, E. C. Tai, D. T. Ting, M. S.
390 Lawrence, W. Haas, N. J. Dyson, A Code of Mono-phosphorylation Modulates the
391 Function of RB. *Mol Cell*. **73**, 985-1000.e6 (2019).

392 10. E. Zatulovskiy, S. Zhang, D. F. Berenson, B. R. Topacio, J. M. Skotheim, Cell growth
393 dilutes the cell cycle inhibitor Rb to trigger cell division. *Science*. **369**, 466–471 (2020).

394 11. S. Zhang, E. Zatulovskiy, J. Arand, J. Sage, J. M. Skotheim, The cell cycle inhibitor RB is
395 diluted in G1 and contributes to controlling cell size in the mouse liver (2022), p.
396 2022.06.08.495371, , doi:10.1101/2022.06.08.495371.

397 12. B. R. Topacio, E. Zatulovskiy, S. Cristea, S. Xie, C. S. Tambo, S. M. Rubin, J. Sage, M.
398 Kõivomägi, J. M. Skotheim, Cyclin D-Cdk4,6 Drives Cell-Cycle Progression via the
399 Retinoblastoma Protein's C-Terminal Helix. *Mol Cell*. **74**, 758-770.e4 (2019).

400 13. S. L. Spencer, S. D. Cappell, F.-C. Tsai, K. W. Overton, C. L. Wang, T. Meyer, The
401 proliferation-quiescence decision is controlled by a bifurcation in CDK2 activity at mitotic
402 exit. *Cell*. **155**, 369–383 (2013).

403 14. M. C. Lanz, E. Zatulovskiy, M. P. Swaffer, L. Zhang, I. Ilerten, S. Zhang, D. S. You, G.
404 Marinov, P. McAlpine, J. E. Elias, J. M. Skotheim, Increasing cell size remodels the
405 proteome and promotes senescence (2021), p. 2021.07.29.454227, ,
406 doi:10.1101/2021.07.29.454227.

407 15. A. Sakaue-Sawano, H. Kurokawa, T. Morimura, A. Hanyu, H. Hama, H. Osawa, S.
408 Kashiwagi, K. Fukami, T. Miyata, H. Miyoshi, T. Imamura, M. Ogawa, H. Masai, A.
409 Miyawaki, Visualizing Spatiotemporal Dynamics of Multicellular Cell-Cycle Progression.
410 *Cell*. **132**, 487–498 (2008).

411 16. C. Xia, J. Fan, G. Emanuel, J. Hao, X. Zhuang, Spatial transcriptome profiling by MERFISH
412 reveals subcellular RNA compartmentalization and cell cycle-dependent gene expression.
413 *Proceedings of the National Academy of Sciences*. **116**, 19490–19499 (2019).

414 17. J. R. Burke, T. J. Liban, T. Restrepo, H.-W. Lee, S. M. Rubin, Multiple Mechanisms for E2F
415 Binding Inhibition by Phosphorylation of the Retinoblastoma Protein C-Terminal Domain.
416 *Journal of Molecular Biology*. **426**, 245–255 (2014).

417 18. F. Dang, L. Nie, J. Zhou, K. Shimizu, C. Chu, Z. Wu, A. Fassl, S. Ke, Y. Wang, J. Zhang, T.
418 Zhang, Z. Tu, H. Inuzuka, P. Sicinski, A. J. Bass, W. Wei, Inhibition of CK1ε potentiates
419 the therapeutic efficacy of CDK4/6 inhibitor in breast cancer. *Nat Commun*. **12**, 5386
420 (2021).

421 19. M. V. Repetto, M. J. Winters, A. Bush, W. Reiter, D. M. Hollenstein, G. Ammerer, P. M.
422 Pryciak, A. Colman-Lerner, CDK and MAPK Synergistically Regulate Signaling Dynamics
423 via a Shared Multi-site Phosphorylation Region on the Scaffold Protein Ste5. *Molecular*
424 *Cell*. **69**, 938-952.e6 (2018).

425 20. E. S. Knudsen, J. Y. Wang, Dual mechanisms for the inhibition of E2F binding to RB by
426 cyclin-dependent kinase-mediated RB phosphorylation. *Mol Cell Biol*. **17**, 5771–5783
427 (1997).

428 21. V. D. Brown, R. A. Phillips, B. L. Gallie, Cumulative Effect of Phosphorylation of pRB on
429 Regulation of E2F Activity. *Mol Cell Biol*. **19**, 3246–3256 (1999).

430 22. R. J. Deshaies, E. D. Emberley, A. Saha, Control of cullin-ring ubiquitin ligase activity by
431 nedd8. *Subcell Biochem*. **54**, 41–56 (2010).

432 23. Z. Luo, Y. Pan, L. S. Jeong, J. Liu, L. Jia, Inactivation of the Cullin (CUL)-RING E3 ligase
433 by the NEDD8-activating enzyme inhibitor MLN4924 triggers protective autophagy in
434 cancer cells. *Autophagy*. **8**, 1677–1679 (2012).

435 24. P. Sdek, H. Ying, H. Zheng, A. Margulis, X. Tang, K. Tian, Z.-X. J. Xiao, The central acidic
436 domain of MDM2 is critical in inhibition of retinoblastoma-mediated suppression of E2F
437 and cell growth. *J Biol Chem*. **279**, 53317–53322 (2004).

25. P. Sdek, H. Ying, D. L. F. Chang, W. Qiu, H. Zheng, R. Touitou, M. J. Allday, Z.-X. J. Xiao, MDM2 Promotes Proteasome-Dependent Ubiquitin-Independent Degradation of Retinoblastoma Protein. *Molecular Cell*. **20**, 699–708 (2005).

26. T. Tomita, J. M. Huibregtse, A. Matouschek, A masked initiation region in retinoblastoma protein regulates its proteasomal degradation. *Nat Commun*. **11**, 2019 (2020).

27. Y. Wang, Z. Zheng, J. Zhang, Y. Wang, R. Kong, J. Liu, Y. Zhang, H. Deng, X. Du, Y. Ke, A Novel Retinoblastoma Protein (RB) E3 Ubiquitin Ligase (NRBE3) Promotes RB Degradation and Is Transcriptionally Regulated by E2F1 Transcription Factor *. *Journal of Biological Chemistry*. **290**, 28200–28213 (2015).

28. S. N. Boyer, D. E. Wazer, V. Band, E7 Protein of Human Papilloma Virus-16 Induces Degradation of Retinoblastoma Protein through the Ubiquitin-Proteasome Pathway1. *Cancer Research*. **56**, 4620–4624 (1996).

29. C. Uchida, S. Miwa, K. Kitagawa, T. Hattori, T. Isobe, S. Otani, T. Oda, H. Sugimura, T. Kamijo, K. Ookawa, H. Yasuda, M. Kitagawa, Enhanced Mdm2 activity inhibits pRB function via ubiquitin-dependent degradation. *EMBO J*. **24**, 160–169 (2005).

30. H. Liu, J. Wang, Y. Liu, L. Hu, C. Zhang, B. Xing, X. Du, Human U3 protein14a is a novel type ubiquitin ligase that binds RB and promotes RB degradation depending on a leucine-rich region. *Biochimica et Biophysica Acta (BBA) - Molecular Cell Research*. **1865**, 1611–1620 (2018).

31. E. Sun, P. Zhang, RNF12 Promotes Glioblastoma Malignant Proliferation via Destructing RB1 and Regulating MAPK Pathway. *J Healthc Eng*. **2021**, 4711232 (2021).

32. A. de Vivo, A. Sanchez, J. Yegres, J. Kim, S. Emly, Y. Kee, The OTUD5–UBR5 complex regulates FACT-mediated transcription at damaged chromatin. *Nucleic Acids Research*. **47**, 729–746 (2019).

33. T. Gudjonsson, M. Altmeyer, V. Savic, L. Toledo, C. Dinant, M. Grøfte, J. Bartkova, M. Poulsen, Y. Oka, S. Bekker-Jensen, N. Mailand, B. Neumann, J.-K. Heriche, R. Shearer, D. Saunders, J. Bartek, J. Lukas, C. Lukas, TRIP12 and UBR5 Suppress Spreading of Chromatin Ubiquitylation at Damaged Chromosomes. *Cell*. **150**, 697–709 (2012).

34. J. M. Tsai, J. D. Aguirre, Y.-D. Li, J. Brown, V. Focht, L. Kater, G. Kempf, B. Sandoval, S. Schmitt, J. C. Rutter, P. Galli, C. R. Sandate, J. A. Cutler, C. Zou, K. A. Donovan, R. J. Lumpkin, S. Cavadini, P. M. C. Park, Q. Sievers, C. Hatton, E. Ener, B. D. Regalado, M. T. Sperling, M. Słabicki, J. Kim, R. Zon, Z. Zhang, P. G. Miller, R. Belizaire, A. S. Sperling, E. S. Fischer, R. Irizarry, S. A. Armstrong, N. H. Thomä, B. L. Ebert, UBR5 forms ligand-dependent complexes on chromatin to regulate nuclear hormone receptor stability. *Molecular Cell*. **0** (2023), doi:10.1016/j.molcel.2023.06.028.

35. K. G. Mark, S. Kolla, J. D. Aguirre, D. M. Garshott, S. Schmitt, D. L. Haakonsen, C. Xu, L. Kater, G. Kempf, B. Martínez-González, D. Akopian, S. K. See, N. H. Thomä, M. Rapé,

475 Orphan quality control shapes network dynamics and gene expression. *Cell*. **0** (2023),
476 doi:10.1016/j.cell.2023.06.015.

477 36. H. Azuma, N. Paulk, A. Ranade, C. Dorrell, M. Al-Dhalimy, E. Ellis, S. Strom, M. A. Kay,
478 M. Finegold, M. Grompe, Robust expansion of human hepatocytes in Fah-/-/Rag2-/-/Il2rg-
479 /- mice. *Nat Biotechnol*. **25**, 903–910 (2007).

480 37. M. Grompe, Fah Knockout Animals as Models for Therapeutic Liver Repopulation. *Adv Exp*
481 *Med Biol*. **959**, 215–230 (2017).

482 38. M. Zhu, T. Lu, Y. Jia, X. Luo, P. Gopal, L. Li, M. Odewole, V. Renteria, A. G. Singal, Y.
483 Jang, K. Ge, S. C. Wang, M. Sorouri, J. R. Parekh, M. P. MacConmara, A. C. Yopp, T.
484 Wang, H. Zhu, Somatic Mutations Increase Hepatic Clonal Fitness and Regeneration in
485 Chronic Liver Disease. *Cell*. **177**, 608-621.e12 (2019).

486 39. L. A. Hehl, D. Horn-Ghetko, J. R. Prabu, R. Vollrath, D. T. Vu, D. A. P. Berrocal, M. P. C.
487 Mulder, G. J. van der H. van Noort, B. A. Schulman, Structural snapshots along K48-linked
488 ubiquitin chain formation by the HECT E3 UBR5 (2023), p. 2023.06.06.543850, ,
489 doi:10.1101/2023.06.06.543850.

490 40. Z. Hodáková, I. Grishkovskaya, H. L. Brunner, D. L. Bolhuis, K. Belačić, A. Schleiffer, H.
491 Kotisch, N. G. Brown, D. Haselbach, Cryo-EM structure of the chain-elongating E3 ligase
492 UBR5 (2022), p. 2022.11.03.515015, , doi:10.1101/2022.11.03.515015.

493 41. F. Wang, Q. He, W. Zhan, Z. Yu, E. Finkin-Groner, X. Ma, G. Lin, H. Li, Structure of the
494 human UBR5 E3 ubiquitin ligase. *Structure*. **31**, 541-552.e4 (2023).

495 42. W. Jiang, S. Wang, M. Xiao, Y. Lin, L. Zhou, Q. Lei, Y. Xiong, K.-L. Guan, S. Zhao,
496 Acetylation regulates gluconeogenesis by promoting PEPCK1 degradation via recruiting
497 the UBR5 ubiquitin ligase. *Mol Cell*. **43**, 33–44 (2011).

498 43. J. M. Suski, M. Braun, V. Strmiska, P. Sicinski, Targeting cell-cycle machinery in cancer.
499 *Cancer Cell*. **39**, 759–778 (2021).

500 44. R. S. Finn, M. Martin, H. S. Rugo, S. Jones, S.-A. Im, K. Gelmon, N. Harbeck, O. N.
501 Lipatov, J. M. Walshe, S. Moulder, E. Gauthier, D. R. Lu, S. Randolph, V. Diéras, D. J.
502 Slamon, Palbociclib and Letrozole in Advanced Breast Cancer. *New England Journal of*
503 *Medicine*. **375**, 1925–1936 (2016).

504 45. G. N. Hortobagyi, S. M. Stemmer, H. A. Burris, Y.-S. Yap, G. S. Sonke, S. Paluch-Shimon,
505 M. Campone, K. L. Blackwell, F. André, E. P. Winer, W. Janni, S. Verma, P. Conte, C. L.
506 Arteaga, D. A. Cameron, K. Petrakova, L. L. Hart, C. Villanueva, A. Chan, E. Jakobsen, A.
507 Nusch, O. Burdaeva, E.-M. Grischke, E. Alba, E. Wist, N. Marschner, A. M. Favret, D.
508 Yardley, T. Bachelot, L.-M. Tseng, S. Blau, F. Xuan, F. Souami, M. Miller, C. Germa, S.
509 Hirawat, J. O'Shaughnessy, Ribociclib as First-Line Therapy for HR-Positive, Advanced
510 Breast Cancer. *N Engl J Med*. **375**, 1738–1748 (2016).

511 46. C. J. Sherr, D. Beach, G. I. Shapiro, Targeting CDK4 and CDK6: From Discovery to
512 Therapy. *Cancer Discovery*. **6**, 353–367 (2016).

513 47. A. C. Garrido-Castro, S. Goel, CDK4/6 Inhibition in Breast Cancer: Mechanisms of
514 Response and Treatment Failure. *Curr Breast Cancer Rep*. **9**, 26–33 (2017).

515 48. L. M. Spring, S. A. Wander, F. Andre, B. Moy, N. C. Turner, A. Bardia, Cyclin-dependent
516 kinase 4 and 6 inhibitors for hormone receptor-positive breast cancer: past, present, and
517 future. *The Lancet*. **395**, 817–827 (2020).

518 49. M. Malumbres, R. Sotillo, D. Santamaría, J. Galán, A. Cerezo, S. Ortega, P. Dubus, M.
519 Barbacid, Mammalian cells cycle without the D-type cyclin-dependent kinases Cdk4 and
520 Cdk6. *Cell*. **118**, 493–504 (2004).

521 50. K. Kozar, M. A. Ciemerych, V. I. Rebel, H. Shigematsu, A. Zagozdzon, E. Sicinska, Y.
522 Geng, Q. Yu, S. Bhattacharya, R. T. Bronson, K. Akashi, P. Sicinski, Mouse development
523 and cell proliferation in the absence of D-cyclins. *Cell*. **118**, 477–491 (2004).

524 51. C. Liu, Y. Konagaya, M. Chung, L. H. Daigh, Y. Fan, H. W. Yang, K. Terai, M. Matsuda, T.
525 Meyer, Altered G1 signaling order and commitment point in cells proliferating without
526 CDK4/6 activity. *Nat Commun*. **11**, 5305 (2020).

527 52. A. Regev, S. A. Teichmann, E. S. Lander, I. Amit, C. Benoist, E. Birney, B. Bodenmiller, P.
528 Campbell, P. Carninci, M. Clatworthy, H. Clevers, B. Deplancke, I. Dunham, J. Eberwine,
529 R. Eils, W. Enard, A. Farmer, L. Fugger, B. Göttgens, N. Hacohen, M. Haniffa, M.
530 Hemberg, S. Kim, P. Klenerman, A. Kriegstein, E. Lein, S. Linnarsson, E. Lundberg, J.
531 Lundeberg, P. Majumder, J. C. Marioni, M. Merad, M. Mhlanga, M. Nawijn, M. Netea, G.
532 Nolan, D. Pe'er, A. Phillipakis, C. P. Ponting, S. Quake, W. Reik, O. Rozenblatt-Rosen, J.
533 Sanes, R. Satija, T. N. Schumacher, A. Shalek, E. Shapiro, P. Sharma, J. W. Shin, O.
534 Stegle, M. Stratton, M. J. T. Stubbington, F. J. Theis, M. Uhlen, A. van Oudenaarden, A.
535 Wagner, F. Watt, J. Weissman, B. Wold, R. Xavier, N. Yosef, Human Cell Atlas Meeting
536 Participants, The Human Cell Atlas. *eLife*. **6**, e27041 (2017).

537 53. K. J. Abraham, N. Khosraviani, J. N. Y. Chan, A. Gorthi, A. Samman, D. Y. Zhao, M.
538 Wang, M. Bokros, E. Vidya, L. A. Ostrowski, R. Oshidari, V. Pietrobon, P. S. Patel, A.
539 Algouneh, R. Singhania, Y. Liu, V. T. Yerlici, D. D. De Carvalho, M. Ohh, B. C. Dickson,
540 R. Hakem, J. F. Greenblatt, S. Lee, A. J. R. Bishop, K. Mekhail, Nucleolar RNA
541 polymerase II drives ribosome biogenesis. *Nature*. **585**, 298–302 (2020).

542 54. M. Charni-Natan, I. Goldstein, Protocol for Primary Mouse Hepatocyte Isolation. *STAR*
543 *Protoc*. **1**, 100086 (2020).

544 55. Y. Jin, T. Anbarchian, P. Wu, A. Sarkar, M. Fish, W. C. Peng, R. Nusse, Wnt signaling
545 regulates hepatocyte cell division by a transcriptional repressor cascade. *Proceedings of the*
546 *National Academy of Sciences*. **119**, e2203849119 (2022).

547 56. D. F. Berenson, E. Zatulovskiy, S. Xie, J. M. Skotheim, Constitutive expression of a
548 fluorescent protein reports the size of live human cells. *MBoC*. **30**, 2985–2995 (2019).

57. C. Lucchesi, S. Mohibi, X. Chen, Measuring Translation Efficiency by RNA Immunoprecipitation of Translation Initiation Factors. *Methods Mol Biol*. **2267**, 73–79 (2021).

58. X. Liu, J. Yan, M. W. Kirschner, Beyond G1/S regulation: how cell size homeostasis is tightly controlled throughout the cell cycle? (2022), p. 2022.02.03.478996, , doi:10.1101/2022.02.03.478996.

Acknowledgements

We thank Julien Sage, Seth Rubin, Hao Zhu, Peter Pryciak and members of the Skotheim laboratory for discussions and feedback on the manuscript. We thank Hao Zhu for sharing the *Fah* transposon plasmids. We thank Markus Grompe for sharing the *Fah-/-* mice. This work was supported by a Chan Zuckerberg Biohub Investigator Award (J.M.S.), and the NIH (P01 CA254867 and K99GM147351). The siRNA screens were done using the ImageXpress Micro CONFOCAL microscope at the High Throughput Screening Knowledge Center (HTSKC) at Stanford, which was funded by the NIH Shared Instrumentation Grant (S10OD026899).

Author contributions

S.Z. performed the experiments, L.V. performed the mathematical modeling, E.Z., S.Z, and J.M.S. designed the experiments, and S.Z. and J.M.S. wrote the manuscript.

Competing interests

The authors declare no competing interest.

Supplementary Materials

Materials and Methods

Figs. S1 to S11

Table S1

580 **Figures and Figure captions**

581

582 **Fig. 1**

583

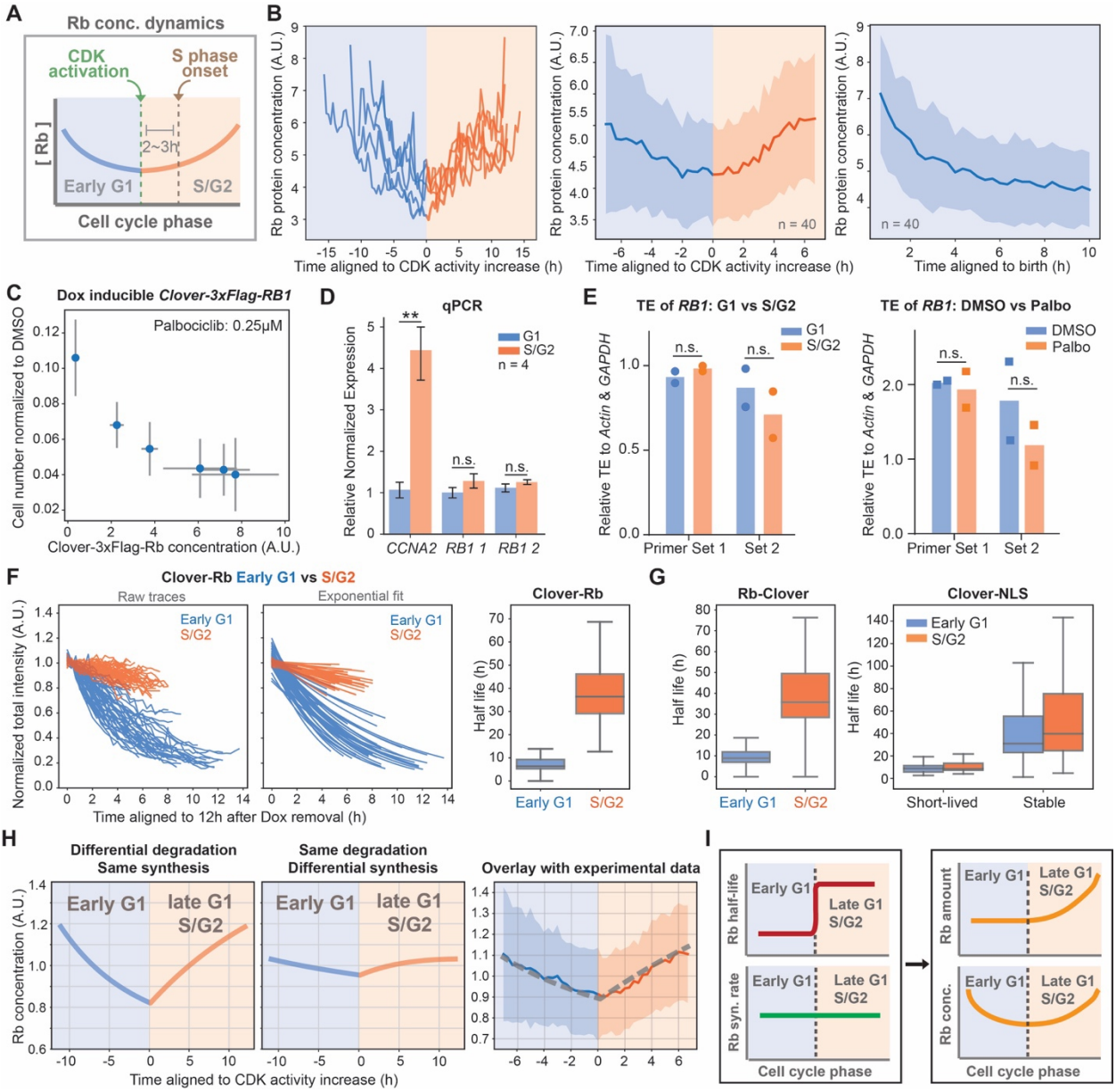

584

585

586

587 **Fig. 1. Rb concentration dynamics are determined by degradation in early- to mid-G1**
588 **A.** Schematic illustration of Rb concentration dynamics through the cell cycle. CDK activation
589 occurs 2-3 hours before the initiation of DNA replication (*1*, *10*). **B**. Fluorescent traces from
590 HMEC-hTERT1 cells expressing endogenously tagged *RB1-3xFLAG-Clover-sfGFP* and the
591 HDHB CDK sensor [1] (n = 40). Left panel shows representative single-cell traces and the middle
592 and right panels show average traces with shaded regions indicating the standard deviation.
593 Traces are aligned either by the initial translocation of the HDHB CDK sensor (middle panel) or
594 cell birth (right panel). **C.** Normalized cell number of HMEC cells treated with either DMSO or
595 Palbociclib (0.25μM) for 72 hours. Cells were plated in media containing different doses of
596 doxycycline to induce exogenous Clover-3xFlag-Rb. Drug treatment started the next day and
597 lasted for 72 hours. Then, cells were fixed and the cell number in each well was measured.
598 Normalized cell number is the cell number under Palbociclib treatment divided by the cell
599 number under DMSO treatment. N = 3 biological replicates, the error bar indicates standard
600 deviation. **D.** qPCR (n = 4) measurements of the *RB1* mRNA concentration in G1 and S/G2
601 HMEC cells sorted using a FUCCI cell cycle reporter. **E.** Translation efficiency (TE) of *RB1* was
602 determined in HMEC cells in G1 and S/G2 that had been sorted using a FUCCI marker (left
603 panel), and in HMEC cells treated with DMSO or Palbociclib (1μM) (right panel). TE was
604 measured using a RIP assay (RNA binding protein immunoprecipitation) by pulling down eIF4E.
605 TE is calculated by dividing the eIF4E bound fraction of *RB1* mRNA to the eIF4E bound
606 fraction of *GAPDH & Actin* mRNAs. Bars denote mean values and dots denote each replicate
607 experiment. **F.** (Left panel) The degradation traces of Clover-3xFlag-Rb protein after Dox
608 withdrawal. The traces were classified into early G1 phase or S/G2 phase based on a FUCCI cell
609 cycle marker and cell cycle phase duration. (Middle panel) The exponential fit of the degradation
610 traces. (Right panel) Distribution of half-lives estimated from the exponential fit. Box plot
611 indicates 5th, 25th, median, 75th and 95th percentiles. **G.** Same half-life measurement as in panel
612 F, but using a C-terminally tagged Rb-3xFlag-Clover (Left panel) or a short-lived Clover-NLS or
613 stable Clover-NLS (Right panel). **H.** Mathematical model of Rb concentration dynamics during
614 cell cycle progression (see methods). Left panel: Rb concentration dynamics assuming that its
615 degradation rate decreases by 80% at the G1/S transition as measured by live imaging (see panel
616 F) and its synthesis rate does not change (left panel), or if Rb's degradation rate does not change,
617 but its synthesis rate increases by 20% at the G1/S transition as measured in panel D. Right panel
618 shows the overlay of the model based on regulated Rb degradation with the experimental data
619 from panel B (middle panel). Rb concentration is normalized to the mean. **I.** Model schematic:
620 differential degradation of Rb in G1 and S/G2 phases of the cell cycle drive its concentration
621 dynamics.
622

Fig. 2

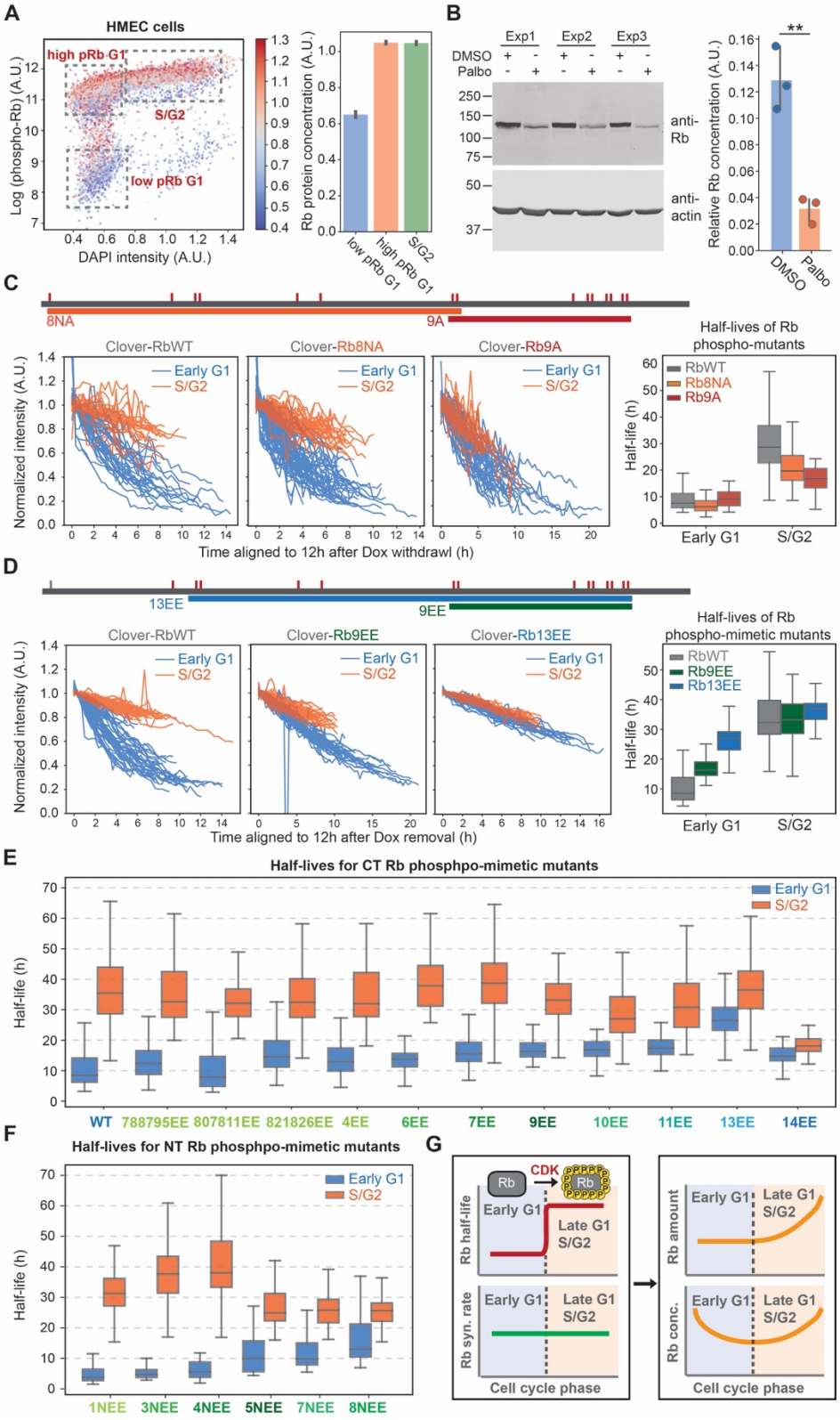
A
HMEC cells
high pRb G1
S/G2
low pRb G1
Log (phospho-Rb) (A.U.)
DAPI intensity (A.U.)
Rb protein concentration (A.U.)
low pRb G1
high pRb G1
S/G2
B
Exp1
Exp2
Exp3
DMSO
Palbo
anti-Rb
anti-actin
Relative Rb concentration (A.U.)
DMSO
Palbo
C
8NA
9A
Clover-RbWT
Clover-Rb8NA
Clover-Rb9A
Early G1
S/G2
Normalized intensity (A.U.)
Time aligned to 12h after Dox withdrawl (h)
Half-lives of Rb phospho-mutants
RbWT
Rb8NA
Rb9A
Half-life (h)
Early G1
S/G2
D
13EE
9EE
Clover-RbWT
Clover-Rb9EE
Clover-Rb13EE
Early G1
S/G2
Normalized intensity (A.U.)
Time aligned to 12h after Dox removal (h)
Half-lives of Rb phospho-mimetic mutants
RbWT
Rb9EE
Rb13EE
Half-life (h)
Early G1
S/G2
E
Half-lives for CT Rb phosphpo-mimetic mutants
Early G1
S/G2
Half-life (h)
WT
788795EE
807811EE
821826EE
4EE
6EE
7EE
9EE
10EE
11EE
13EE
14EE
F
Half-lives for NT Rb phosphpo-mimetic mutants
Early G1
S/G2
Half-life (h)
1NEE
3NEE
4NEE
5NEE
7NEE
8NEE
G
Rb
CDK
Rb half-life
Early G1
Late G1
S/G2
Rb syn. rate
Cell cycle phase
Rb amount
Rb conc.

627 **Fig. 2. Rb protein is stabilized via phosphorylation by Cyclin-Cdk**
628 **A.** Rb concentration in different phospho-Rb populations. HMEC cells were stained with
629 phospho-Rb (S807/811) antibody and Rb antibody. (Left panel) phospho-Rb intensity is plotted
630 against DNA content (DAPI intensity). The color indicates Rb concentration. (Right panel)
631 quantification Rb concentrations in different phospho-Rb populations as shown in the boxes in
632 the left panel. Bar plots indicate the mean and 95% confidence interval. **B.** Immunoblot of Rb
633 after DMSO or Palbociclib (1μM) treatment for 24 hours. The quantification of relative Rb
634 concentration (normalized to actin intensity) is shown on the right. **C.** Top panel shows the
635 schematic of Rb phospho-site mutants. Small red lines indicate the location of Cdk
636 phosphorylation sites. Lower panel shows the degradation traces for Clover-3xFlag-RbWT,
637 Clover-3xFlag-Rb8NA, and Clover-3xFlag-Rb9A as well as the corresponding distributions of
638 half-lives. **D.** Top panel shows the schematic of the Rb phospho-mimetic mutants. Lower panel
639 shows the degradation traces for Clover-3xFlag-RbWT, Clover-3xFlag-Rb9EE, and Clover-
640 3xFlag-Rb13EE, as well as the corresponding distributions of half-lives. **E-F.** Half-life
641 distributions for all the Rb phospho-mimetic mutants. **G.** Model schematic: Rb is stabilized in
642 late G1 and S/G2 phases by Cdk phosphorylation.
643

Fig. 3

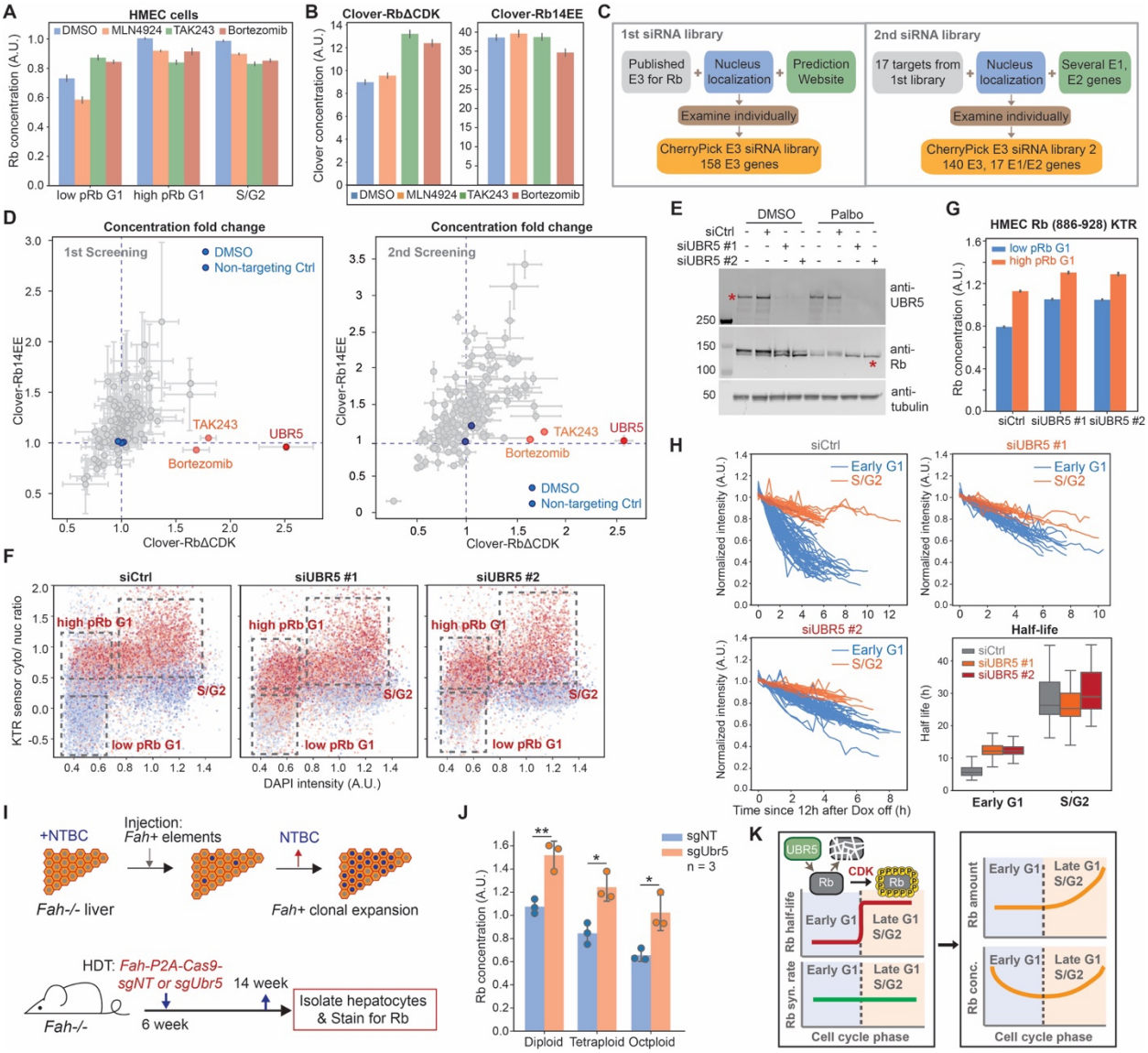
A
HMEC cells
DMSO MLN4924 TAK243 Bortezomib
Rb concentration (A.U.)
low pRb G1
high pRb G1
S/G2
B
Clover-RbΔCDK
Clover-Rb14EE
Clover concentration (A.U.)
C
1st siRNA library
Published E3 for Rb
Nucleus localization
Prediction Website
Examine individually
CherryPick E3 siRNA library 158 E3 genes
2nd siRNA library
17 targets from 1st library
Nucleus localization
Several E1, E2 genes
Examine individually
CherryPick E3 siRNA library 2 140 E3, 17 E1/E2 genes
D
Concentration fold change
1st Screening
2nd Screening
DMSO
Non-targeting Ctrl
TAK243
UBR5
Bortezomib
Clover-Rb14EE
Clover-RbΔCDK
E
DMSO
Palbo
siCtrl
siUBR5 #1
siUBR5 #2
anti-UBR5
anti-Rb
anti-tubulin
G
HMEC Rb (886-928) KTR
low pRb G1
high pRb G1
Rb concentration (A.U.)
siCtrl
siUBR5 #1
siUBR5 #2
F
siCtrl
siUBR5 #1
siUBR5 #2
KTR sensor cyto/ nuc ratio
high pRb G1
S/G2
low pRb G1
DAPI intensity (A.U.)
H
siCtrl
siUBR5 #1
siUBR5 #2
Early G1
S/G2
Normalized intensity (A.U.)
Time since 12h after Dox off (h)
Half-life
Half life (h)
Early G1
S/G2
I
+NTBC
Injection: Fah+ elements
NTBC
Fah-/- liver
Fah+ clonal expansion
HDT: Fah-P2A-Cas9-sgNT or sgUbr5
14 week
6 week
Fah-/-
Isolate hepatocytes & Stain for Rb
J
sgNT
sgUbr5
n = 3
Rb concentration (A.U.)
Diploid
Tetraploid
Octploid
K
UBR5
Rb
CDK
Rb half-life
Rb syn. rate
Early G1
Late G1 S/G2
Cell cycle phase
Rb amount
Rb conc.

Fig. 3. The degradation of un-phosphorylated Rb is mediated by the E3 ligase UBR5

A. Rb concentration in different phospho-Rb populations of HMEC cells after indicated drug treatments. HMEC cells were treated with the indicated drugs for 5 hours, fixed, and stained with phospho-Rb (S807/811) and Rb antibodies. The Rb concentration is calculated by dividing total Rb intensity by nuclear area$^{3/2}$. **B.** Concentrations of Clover-3xFlag-RbΔCDK or Clover-3xFlag-Rb14EE after drug treatments. Cells expressing Clover-3xFlag-RbΔCDK and Clover-3xFlag-Rb14EE were induced with Dox (1μg/mL) for 48 hours. Then, cells were treated with the indicated drugs for 5 hours, fixed, and imaged. The concentrations of Clover-3xFlag-Rb variants were calculated by dividing total Clover intensity by nuclear area$^{3/2}$. **C.** Schematics of the two siRNA library components. **D.** Results of the two siRNA screens. The concentration fold changes of Clover-3xFlag-RbΔCDK and Clover-3xFlag-Rb14EE are plotted. The concentration fold change is calculated by dividing the Clover concentration of the treatment well by the concentration of the non-treated well. n = 4 biological replicates were performed for the 1st screen, and n = 3 biological replicates were performed for the 2nd screen. **E.** Immunoblot of Rb after UBR5 knockdown by siRNA. Cells were treated with siRNAs for 24 hours, and then treated with DMSO or Palbociclib (1μM) for 24 hours before harvest. The lower band in the Rb blot indicates the un/hypo-phosphorylated Rb (marked by red star). **F.** Microscopy analysis of HMEC cells expressing the Rb (886-928) KTR sensor, which reflects Cdk activity. Cells were treated with Ctrl siRNA or *UBR5* siRNAs for 48 hours. The cytoplasmic-to-nucleus intensity ratio of the KTR sensor is plotted against DNA content (DAPI staining). The dot color indicates the Rb concentration. **G.** Quantification of Rb concentration in different phospho-Rb populations shown in (F). Bars indicate mean and its 95% confidence interval. **H.** Degradation traces and the calculated half-lives of Clover-3xFlag-Rb after *UBR5* knock down. Box plot indicates 5th, 25th, median, 75th and 95th percentiles. **I.** Schematic of the *Fah-/-* mouse liver model and experimental flow. 6-week old *Fah-/-* mice were hydrodynamically transfected with plasmids carrying an *Fah-P2A-Cas9-sgNT* transposon or an *Fah-P2A-Cas9-sgUbr5* transposon, together with a transposase plasmid. 8 weeks later, hepatocytes were isolated from the mice for downstream analysis. **J.** Rb concentration in the low-phospho-Rb population of the primary hepatocytes isolated from mice receiving *Fah-P2A-Cas9-sgNT* or *Fah-P2A-Cas9-sgUbr5* transposons. The error bars indicate the standard deviation of the mean. **K.** Model schematic: Un-phosphorylated Rb is targeted for degradation by the E3 ligase UBR5 in early G1.

681 **Fig. 4**

682

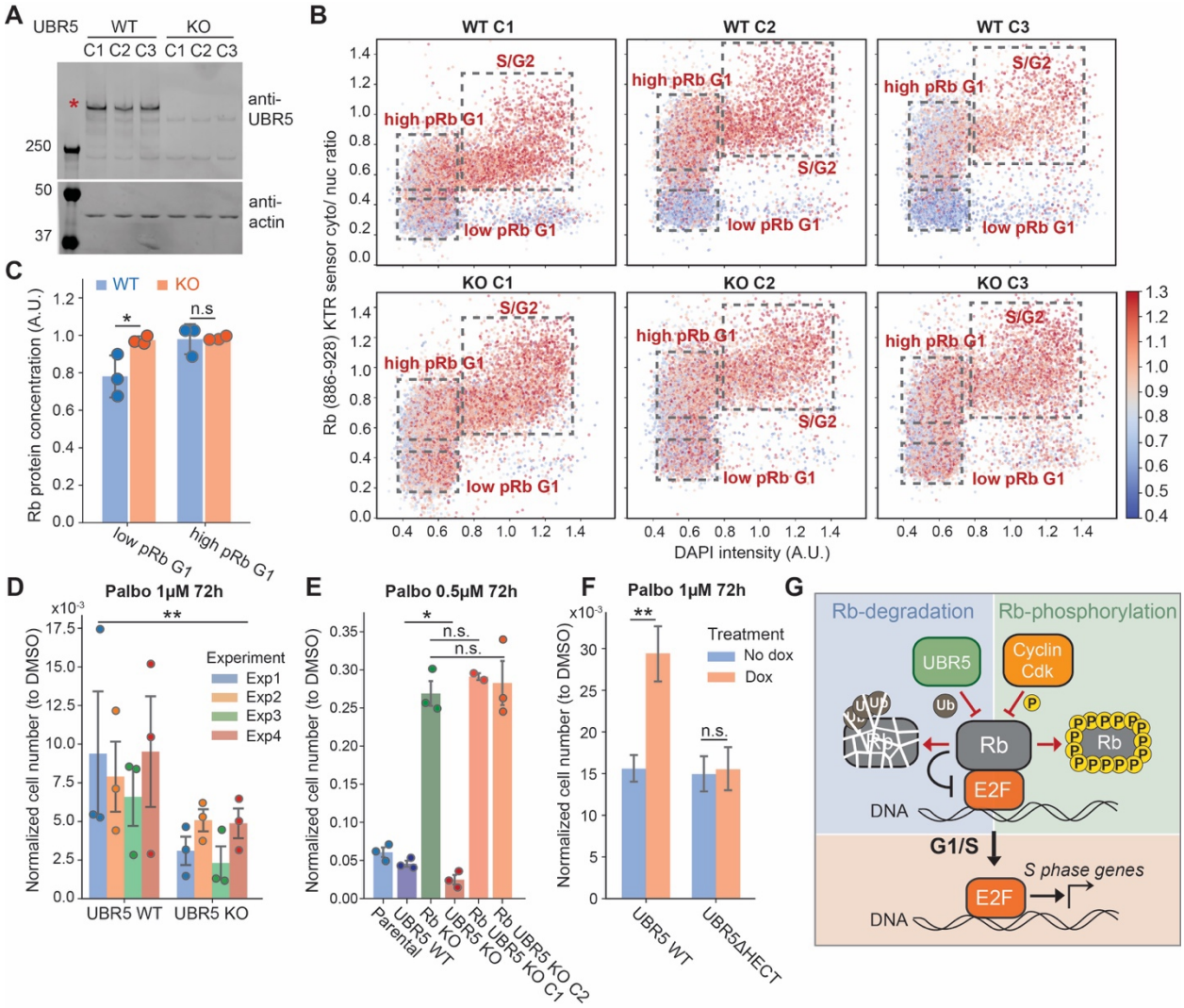

683

684

685 **Fig. 4. UBR5 deletion sensitizes cells to CDK4/6 inhibition**
686 **A.** Immunoblot verification of *UBR5 KO* clonal cell lines. **B.** Rb staining in *UBR5 WT* or *KO*
687 clonal cell lines expressing the Rb (886-928) KTR sensor. The cytoplasmic-to-nucleus intensity
688 ratio of the KTR sensor is plotted against DNA content (DAPI staining). The dot color indicates
689 the Rb concentration. **C.** Quantification of Rb concentration in different phospho-Rb populations
690 shown in (b). Circles denote results from individual clones and the bars denote the standard
691 deviation. **D.** Normalized cell number of *UBR5 WT* or *KO* clonal cell lines after Palbociclib
692 (1μM) treatment for 72 hours. Drug treatment started the day after plating. After 72 hours of
693 drug treatment, cells were fixed and the cell number in each well was measured. Normalized cell
694 number is the cell number under Palbociclib treatment divided by the cell number under DMSO
695 control treatment. N = 4 biological replicates and error bars indicate the standard deviation. **E.**
696 Normalized cell number of *UBR5 WT*, *RB1 KO*, or *RB1 UBR5* double *KO* clonal cell lines after
697 Palbociclib (0.5μM) treatment for 72 hours. N = 3 biological replicates. **F.** Normalized cell
698 number of UBR5 WT addback or UBR5ΔHECT addback cells after Palbociclib (1μM) treatment
699 for 72 hours. GFP-UBR5 WT or GFP-UBR5ΔHECT were induced by Dox (100ng/ml). The
700 results show the average from 3 *UBR5 KO* clonal cell lines with different UBR5 variants added
701 back. We performed 3 biological replicates. The error bars indicate the standard deviation. **G.**
702 Model schematic showing Rb is targeted for degradation by UBR5 in parallel to the canonical
703 Rb phosphorylation pathway controlling Rb activity and thereby the G1/S transition.
704
705